AD_____

Award Number: DAMD17-03-1-0558

TITLE: Development and Characterization of Novel Volumetric Acquisition Orbits with an Application Specific Emission Tomograph for Improved Breast Cancer Detection

PRINCIPAL INVESTIGATOR: Kristy Perez
Caryl N. Brzymialkiewicz (Archer)

CONTRACTING ORGANIZATION: Duke University
Durham, NC 27710

REPORT DATE: August 2007

TYPE OF REPORT: Annual Summary

PREPARED FOR: U.S. Army Medical Research and Materiel Command
Fort Detrick, Maryland 21702-5012

REPORT DOCUMENTATION PAGE

Form Approved
OMB No. 0704-0188

1. REPORT DATE	2. REPORT TYPE	3. DATES COVERED
01-08-2007	Annual Summary	14 Jul 2006 – 13 Jul 2007

4. TITLE AND SUBTITLE

Development and Characterization of Novel Volumetric Acquisition Orbits with an Application Specific Emission Tomograph for Improved Breast Cancer Detection

5a. CONTRACT NUMBER

5b. GRANT NUMBER
DAMD17-03-1-0558

5c. PROGRAM ELEMENT NUMBER

6. AUTHOR(S)

Kristy Perez
Caryl N. Brzymialkiewicz (Archer)
Email: klp14@duke.edu

5d. PROJECT NUMBER

5e. TASK NUMBER

5f. WORK UNIT NUMBER

7. PERFORMING ORGANIZATION NAME(S) AND ADDRESS(ES)

Duke University
Durham, NC 27710

8. PERFORMING ORGANIZATION REPORT NUMBER

9. SPONSORING / MONITORING AGENCY NAME(S) AND ADDRESS(ES)
U.S. Army Medical Research and Materiel Command
Fort Detrick, Maryland 21702-5012

10. SPONSOR/MONITOR'S ACRONYM(S)

11. SPONSOR/MONITOR'S REPORT NUMBER(S)

12. DISTRIBUTION / AVAILABILITY STATEMENT
Approved for Public Release; Distribution Unlimited

13. SUPPLEMENTARY NOTES

14. ABSTRACT

The overall goal of this work was to develop, implement, and evaluate novel three-dimensional acquisition orbits for a dedicated emission mammotomography system. The system can revolve around a pendant, uncompressed breast with fully three dimensional orbital trajectories, which allow for chest wall and axillary imaging. Further optimization and characterization of the system's flexible trajectories and resulting reconstructed images continues. Upon the recommendations from this and prior work, one patient study has been completed.

15. SUBJECT TERMS
Nuclear Medicine Imaging, SPECT, Dedicated Tomographic Breast Imaging, Mammotomograph

16. SECURITY CLASSIFICATION OF:			17. LIMITATION OF ABSTRACT	18. NUMBER OF PAGES	19a. NAME OF RESPONSIBLE PERSON
a. REPORT	b. ABSTRACT	c. THIS PAGE			USAMRMC
U	U	U	UU	17	19b. TELEPHONE NUMBER *(include area code)*

Table of Contents

Introduction

The overall goal of this work was to develop, implement, and evaluate novel three-dimensional acquisition orbits for a dedicated emission mammotomography system. With the prototype system built and acquisition orbits tested and working, evaluation of the system continues. The graphical user interface (GUI) used to calculate orbits and to create a text file, which directs the camera's motion, has been modified and debugged to increase its speed and capabilities. A contrast-detail analysis determining the minimum detectable lesion size of lesion detectable at differing contrast levels indicates that lesions as small as 3.1mm can be visualized. Angular sampling in the system is being studied and recommendations on the appropriate amount of angular sampling will be made.

Body

Tasks 1 through 2c were completed in Years 1 and 2. The remaining tasks, 2d through 3c have been completed in Year 3 and are described below.

Task 2D *Develop software to automate process of orbit creation, utilizing dynamic ROR control.*
The Orbit Creation GUI has been debugged and modified to allow more versatile control over orbit creation. Functions were added to export and print plots created in the program. Additionally, a table position feature was added to allow input of values for each direction of bed motion (azimuthal, polar and ROR). Previously, an orbital plot had been used where selected points were used to calculate the orbital trajectory. However, the scale on the plot was too large to make this method practical. Using direct table position input in order to develop a fully contoured orbit was found to be much more accurate.

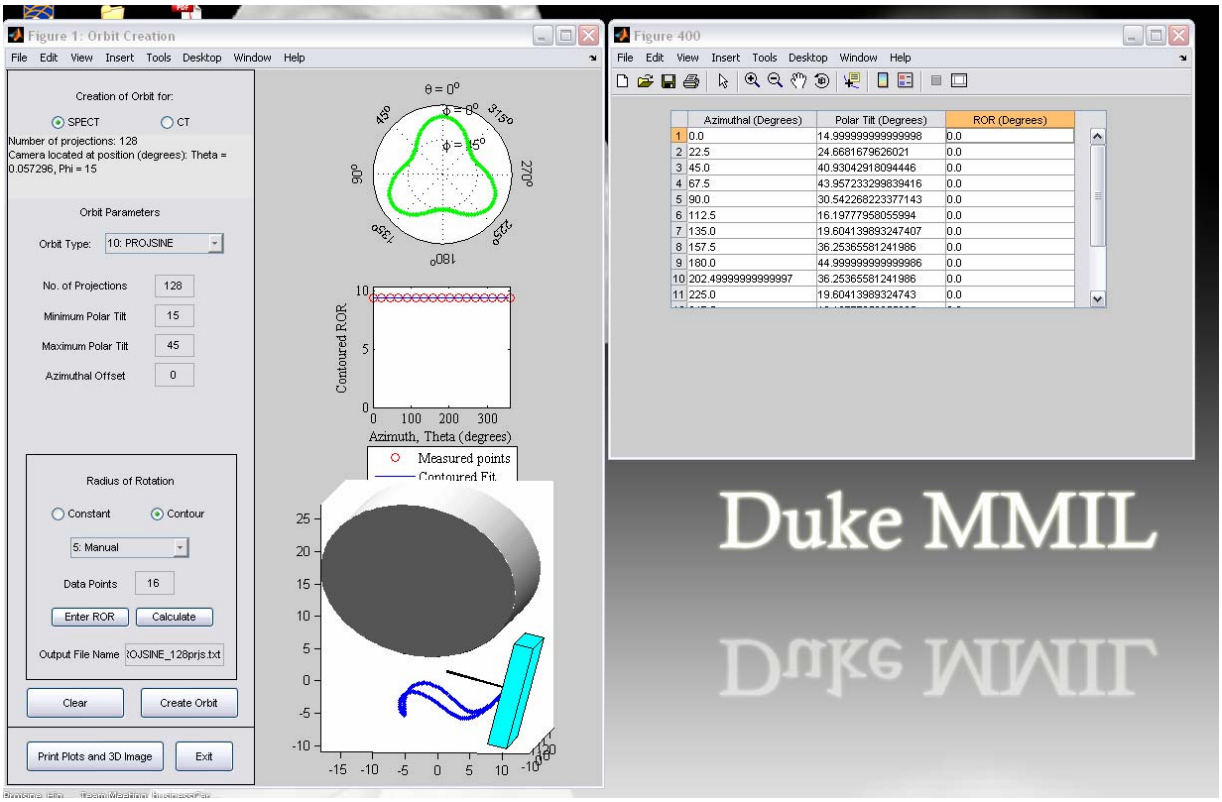

Fig. 1. Screenshot of software for creation of simple or complex orbits. (LEFT) GUI which has the options to select orbit type, designate parameters for polar sampling and enter radius of rotation (ROR). After clicking "Create Orbit" button, the software calculates the orbit and displays the trajectory in three views. (RIGHT) Table to enter ROR positions to fully contour the breast or object in FOV. After measured positions are entered, the program iterates between them to calculate

orbit positions at each projection angle. The number of entered data points can vary, but experimentally we have determined 8 to 12 suffice, depending on the orbit being created and shape of object.

Task 3 *Experimental evaluation of orbits*

Significant progress has been made in the evaluation of acquisition orbits and the resulting effect on reconstructed images characteristics. A contrast versus detail observer study has been performed to determine the smallest hot (radioactive) and cold (non-radioactive) lesions which can be detected for various contrast levels. The detailed methods for this study are provided in Appendix B.

Observers were shown images for a range of concentration ratios and orbits (Figure 2, left). Observer study results indicate that for concentration ratios (rod : background) of 5:1 and 2.5:1 there is a statistically significant difference between the mean detectable limit of a tilted parallel beam (TPB) image versus a projected sine wave (PROJSINE) image, where the smaller lesions can be detected in the TPB image (Figure 2, right). This difference can be explained by understanding that resolution is a function of the distance the detector is from the source. The TPB orbit acquired more projection views closer to the cross section of slices used in the study than the PROJSINE orbit.

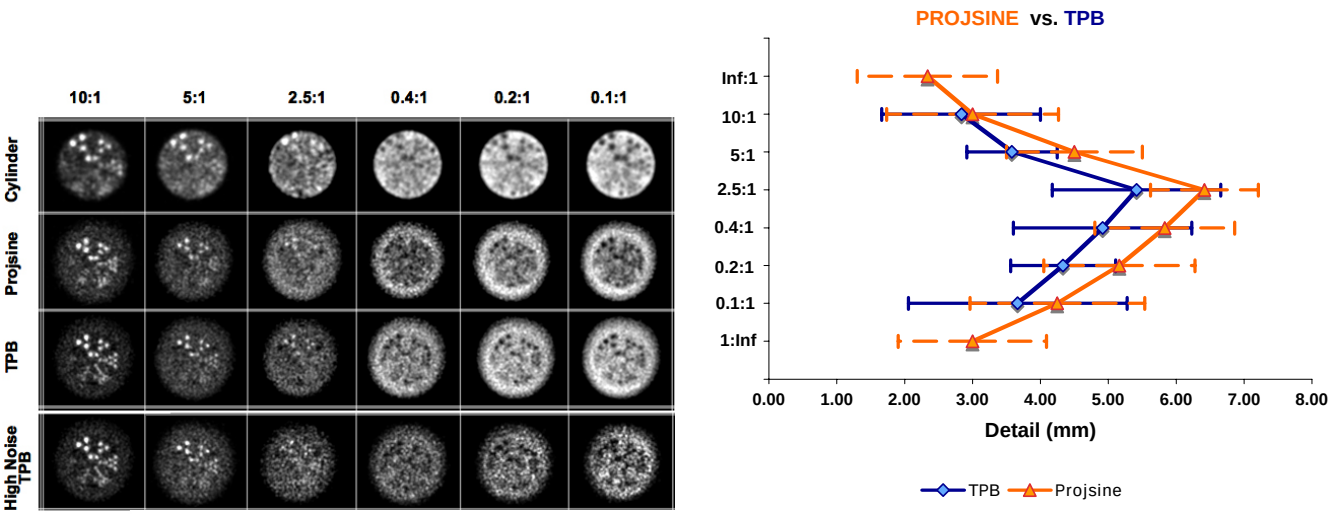

Fig. 2. (LEFT) Reconstructed summed slice images for concentration ratios ranging from 10:1 down to 0.1:1 (effectively 1:10) for circular scans about the cylinder (1st row), and two trajectories about the breast phantom (2nd and 3rd rows). For comparison, the high noise reconstructions for the TPB orbit are shown on the bottom row. The projection count densities were normalized to the 10:1 case, so that the effect of noise in the image could be investigated in the observer study. (RIGHT) Contrast vs. detail comparing PROJSINE to TPB orbits using combined high and low noise observations. There are statistically significant differences in mean values at the contrasts of 5:1 and 2.5:1 at $p<0.05$. For the Inf:1, and 1:Inf concentration ratios, only PROJSINE scans were acquired.

An investigation into the angular sampling dependence of the image has been completed. Previous studies[1] indicated that the number of counts per projection was more important than the total number of projections or possibly the total number of counts in the image. Figures 3 and 4 highlight the results of the study, showing that reconstructed images are very similar when varying the number of projections while keeping counts per projection constant. However, object recovery is degraded when the total acquired counts per acquisition are constant, but divided over a different number of projections. To ensure that all variables except the number of counts per projection or per scan are constant, one data set of projections was down sampled to form the compared images. To produce the reconstructed images with 128 projections, every other projection of the 256 projections was removed. Similarly, to produce the reconstructed image with 64 images every other projection of the 128 was removed. In order to equalize the total counts in the reconstructed images, the number of counts in the each projection of the set of 128 was divided by 2 and of the set of 256 was divided by 4 and thus these

images will have approximately the same total number of counts as the images reconstructed with 64 projections. For display purposes in the following figures, the contrast values are the same in each image.

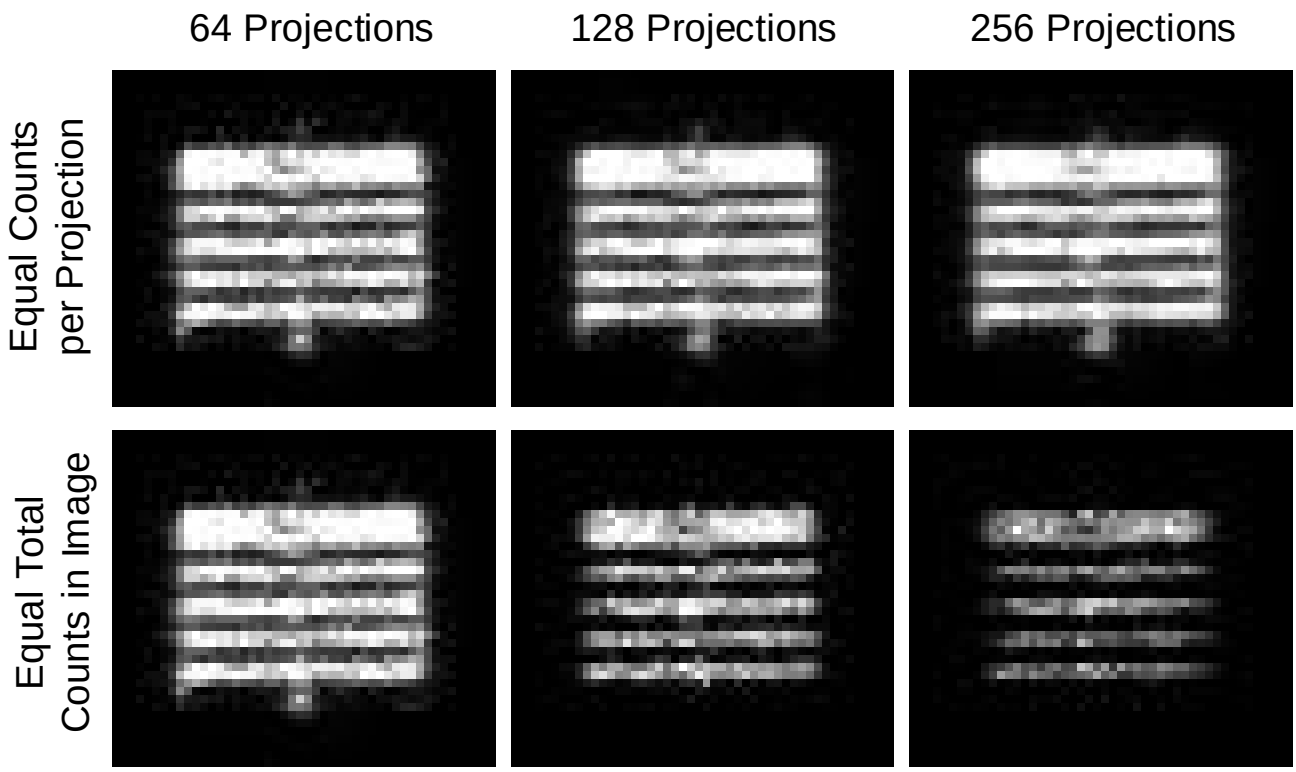

Fig. 3. Comparison of VAOR data set at the same contrast level with varied projection numbers and counts. The top right corner image is the reconstructed image from the originally collected data set. All other images are down sampled versions. (TOP ROW) Reconstructed images formed with 64, 128 and 256 projections. Image reconstructed with 64 and 128 projections are derived by removing slices from the collected data of 256 projections. Qualitatively, these images are very similar. (BOTTOM ROW) Reconstructed images formed with 128 projections and 256 projections are derived by dividing the number of counts per projection by 2 and 4, respectively, to equal the approximate number of total counts in the image formed with 64 projections. The differences in the images are obvious with degradation in the shape of the disks, disappearance of the outer wall of the cylinder phantom and disappearance of the center cylinder of radioactivity.

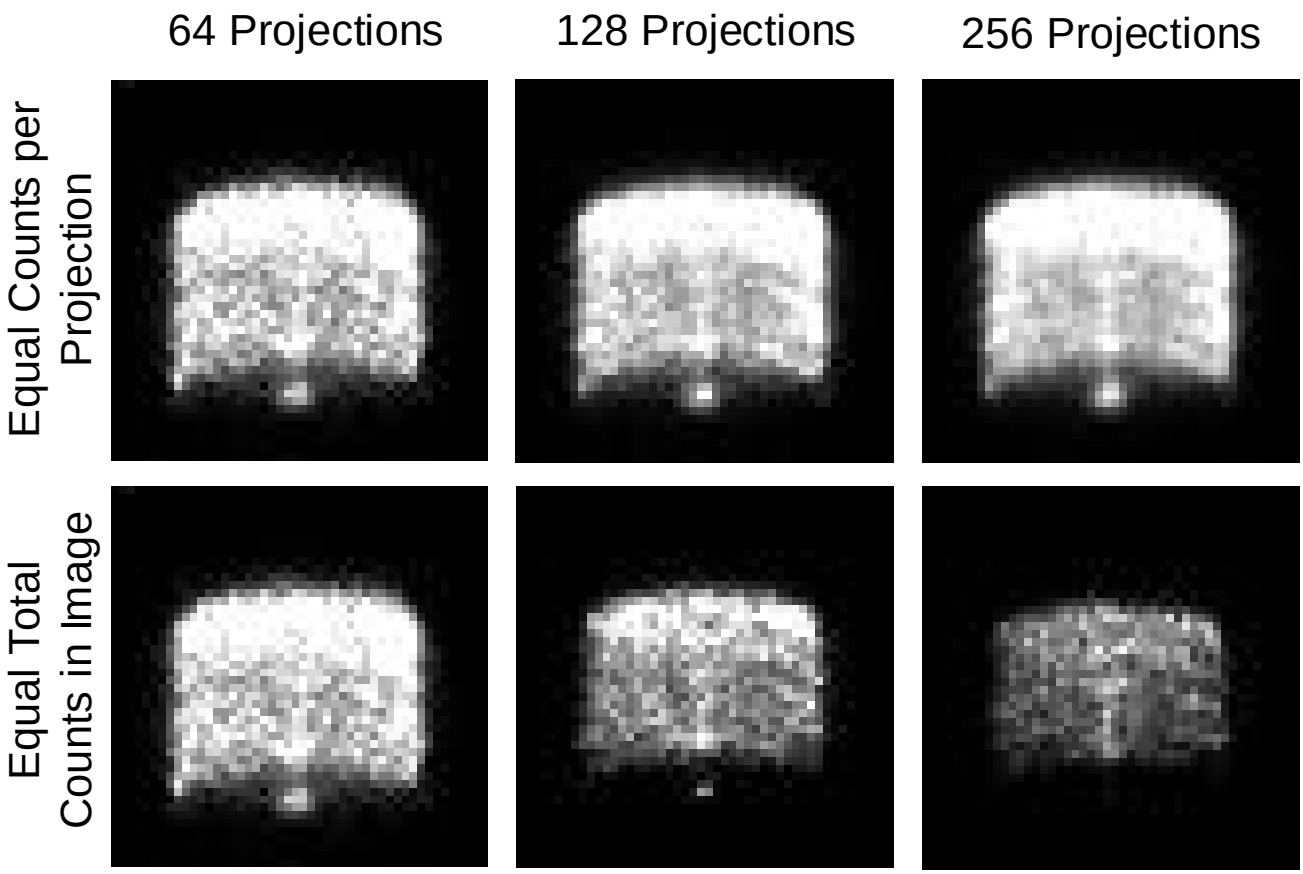

Fig. 4. Comparison of PROJSINE data set at the same contrast level with varied projection numbers and counts. The top right corner image is the reconstructed image from the originally collected data set. All other images are down sampled versions. (TOP ROW) Reconstructed images formed with 64, 128 and 256 projections. Image reconstructed with 64 and 128 projections are derived by removing slices from the collected data of 256 projections. Qualitatively, these images are very similar. (BOTTOM) Reconstructed images formed with 128 projections and 256 projections are derived by dividing the number of counts per projection by 2 and 4, respectively, to equal the approximate number of total counts in the image formed with 64 projections. The differences in the images are obvious with the shrinking of the area of the phantom and disappearance of the center cylinder of radioactivity.

Additionally, the dependence of the spatial frequency of objects being imaged on the quality of the resulting image were explored. A disk phantom was filled with an aqueous solution of ^{99m}Tc and imaged to get a baseline for comparison. Subsequently, acrylic spheres of various sizes were placed between the disks to provide additional spatial frequencies. The first set of data was collected using only 3.5mm diameter spheres. This particular size allowed for two rows of spheres to be hexagonally close packed at approximately the same thickness as the acrylic disks. Another set of data was collected alternating the size of the spheres from 3.5mm to 2.5mm to 5mm between the disks. Results indicate that varying the spatial frequency of non-radioactive objects did not have a visually perceivable effect on the shape of the reconstructed object (Figure 5).

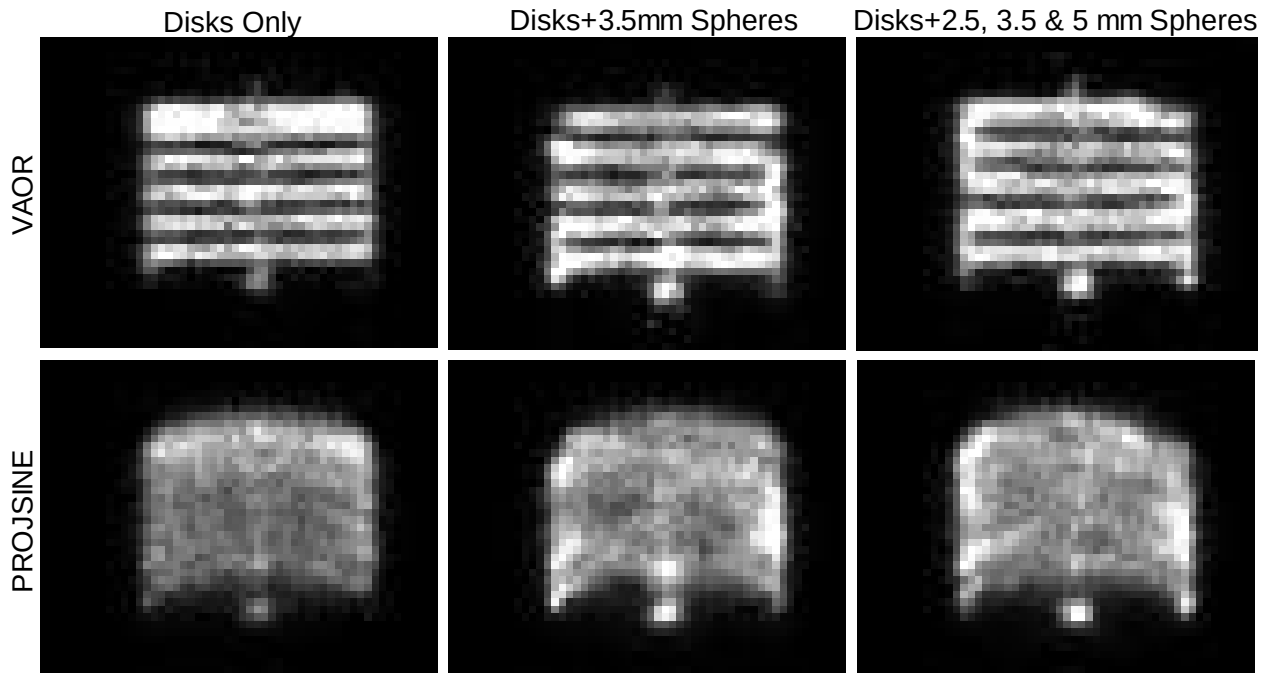

Fig. 5. Reconstructed images of VAOR (top row) and PROJSINE (bottom row) data sets to the same contrast level with disks only (left), disks plus 3.5mm spheres (middle) and disks plus 2.5, 3.5 and 5 mm spheres (right) in an approximately 0.06 mCi/ml ^{99m}Tc aqueous solution. Since the spheres replaced some of the empty volume between the disks, there are areas of higher concentration of the radionuclide than others. Hotspots are seen in both the VAOR and PROJSINE data in approximately the same locations. Also, due to the inclusion of the spheres the edges of the disks appear less smooth in the center and right images. However, the difference in the overall shape between the disk only data set and those with the spheres included is minimal.

Additional experiments are planned to test both the effect of varying the spatial frequency of hot and cold spots and varying the angular sampling.

Key Research Accomplishments

The final year of this project included tasks 2D-3B from the original Statement of Works (Appendix A). A final version of the GUI and software to create orbits has been debugged and thoroughly tested and implemented. Continuing studies of the information gained with different orbits have been and are being done to fully understand the system and its limitations. Summary of Year 3 accomplishments:

- We continue to evaluate and refine the world's first dedicated breast SPECT imaging system
- We have finalized GUI and software to create custom orbits with designated parameters to quickly and efficiently contour objects in the FOV of the detector. This is unique in the realm of nuclear radiology of the breast.
- Refinement of the system through completion of the specific aims of this grant have allowed for the completion of the first known dedicated breast SPECT patient study.
- Results of the first patient study indicate the breast SPECT project has successfully provided a system ready for clinical studies.
- This SPECT system was combined with our developed CT system onto a common gantry, providing the first ever dedicated dual modality SPECT-CT breast imaging system.

Reportable Outcomes

SJ Cutler, **KL Perez**, MP Tornai. "3-D Contrast-Detail Analysis for Dedicated Emission Mammotomography." Presented at the *2006 Nucl. Sci. Symp. & Med. Imag. Conference*, San Diego, CA, 29 Oct. - 4 Nov. 2006, and to be published in *2006 IEEE Nuclear Science Symposium & Medical Imaging Conference Record*.

DJ Crotty, P Madhav, **KL Perez**, SJ Cutler, RL McKinley, T Wong, PK Marcom, MP Tornai. "3-D Molecular Breast Imaging with Dedicated Emission Mammotomography: Results of the First Patient Study." Presented at the *Duke University Center for Molecular and Biomolecular Imaging Meeting*, Durham, NC, 11-13 Mar. 2007.

P Madhav, DJ Crotty, SJ Cutler, **KL Perez**, RL McKinley, MP Tornai. "A Novel Dual-Modality SPECT-CT System Dedicated for 3D Volumetric Breast Imaging." Presented at the *Duke University Center for Molecular and Biomolecular Imaging Meeting*, Durham, NC, 11-13 Mar. 2007.

KL Perez, P Madhav, DJ Crotty, MP Tornai. "Analysis of Patient Bed Positioning in SPECT-CT Imaging for Dedicated Mammotomography." Presented at the *2007 SPIE Medical Imaging Conference*, San Diego, CA, 17-22 Feb. 2007, and published in *Proc. SPIE: Physics of Medical Imaging*.

MP Tornai, P Madhav, DJ Crotty, SJ Cutler, RL McKinley, **KL Perez**, JE Bowsher. "Initial hybrid SPECT-CT system for dedicated fully-3D breast imaging." Presented at *Society of Nuclear Medicine Meeting*, Washington DC, 2-6 June 2007.

MP Tornai, P Madhav, DJ Crotty, SJ Cutler, RL McKinley, **KL Perez**, JE Bowsher. "Application of volumetric molecular breast imaging with a dedicated SPECT-CT mammotomograph." Presented at the *2007 American Association of Physicists in Medicine Meeting*, Minneapolis, MN, 22-26 Jul. 2007.

KL Perez, SJ Cutler, MP Tornai. "Empirical Effects of Angular Sampling and Background Content on Image Quality in Dedicated Breast SPECT." To be presented at the *2007 IEEE Nucl. Sci. Symposium & Med. Imaging Conference*, Honolulu, Hawaii, 28 Oct.-3 Nov. 2007

P Madhav, DJ Crotty, **KL Perez**, SJ Cutler, RL McKinley, T Wong, MP Tornai. "Initial patient study with dedicated dual-modality SPECT-CT mammotomography." To be presented at the *2007 IEEE Nucl. Sci. Symposium & Med. Imaging Conference*, Honolulu, Hawaii, 28 Oct.-3 Nov. 2007

SJ Cutler, DJ Crotty, P Madhav, **KL Perez**, MP Tornai. "Comparison of reduced angle and fully 3D acquisition sequencing and trajectories for dual-modality mammotomography." To be presented at the *2007 IEEE Nucl. Sci. Symposium & Med. Imaging Conference*, Honolulu, Hawaii, 28 Oct.-3 Nov. 2007

Conclusions

With our fully automated system capable of accurate and custom contoured complex orbits, characterization of the images acquired with different detector orbital trajectories has been extensively studied. Studies have shown that lesions as small as 3.1mm can be detected with concentrations as low as 2.5:1. This represents a significant improvement over non-dedicated systems where the smallest detectable lesion size is on the order of 1 cm. Sampling investigations imply that the number of counts per projection rather than the number of projections plays a larger role in object recovery in image reconstruction. Therefore, recommendations on angular sampling and related counts per projection are being made. Experiments investigating effects of spatial frequency are being broadened to include both hot and cold spots to see the effect of varying the size and amount of each. Future work will also include another patient scan on our hybrid SPECT-CT system with our new lead lined patient bed.

References

1. Bryzmialkiewicz, C.N. Development and Evaluation of a Dedicated Emission Mammotomography System. Ph.D. Thesis, Duke University 2005.

APPENDIX A

STATEMENT OF WORK

Task 1 Implement and characterize modified basis set of orbits (Months 1-5):

a. Implement dynamic ROR capability in hardware to enable fully computer controlled gantry. (Month 1)
b. Program gantry for: modified circle-plus-arc orbit with different arc locations, cloverleaf orbit. (Month 2)
c. Perform phantom measurements using modified orbits and evaluate projection data for signal-to-noise (SNR), contrast, and lesion visualization improvement. (Months 2-5).

Task 2 Development and investigation of novel orbits (Months 5-22):

a. Use Monte Carlo and Analytic computer simulations, including computations of Orlov Volumes, to develop novel orbits for various breast shapes and sizes through parameters of viewable breast volume, radius-of-rotation (ROR), camera tilt angle (to minimize background contamination). (Months 5-12)
b. Investigate the effect of additional bed shielding on positioning of the compact gamma camera. (Months 12-15)
c. Investigate acquisition and system parameters, including system tilt for axillary imaging, total number of projections and hence angular sampling, and distribution of the scan time. (Months 15-18)
d. Develop software to automate process of orbit creation, utilizing dynamic ROR control. (Months 18-22)

Task 3 Experimental evaluation of orbits (Months 22-36):

a. Acquire experimental projection data using cold rod and cold disk phantoms for resolution and sampling characterization, respectively. (Months 22-29)
b. Utilize anthropomorphic breast containing lesions and torso phantoms to acquire projection data. Analyze reconstructed images for contrast, signal-to-noise ratio, lesion detectability, and extent of artifacts caused by torso contamination. (Months 29-36)

Appendix B

The following paper was presented at the *2006 Nucl. Sci. Symp. & Med. Imag. Conference*, San Diego, CA, 29 Oct. - 4 Nov. 2006.

3-D Contrast-Detail Analysis for Dedicated Emission Mammotomography

Spencer J. Cutler, *Member, IEEE,* Kristy L. Perez, *Member, IEEE,* and Martin P. Tornai, *Senior Member, IEEE*

Abstract– An observer based 3D contrast-detail study is performed in an effort to evaluate the limits of object detectability for a dedicated CZT-based SPECT mammotomography imaging system under various imaging conditions. A novel, geometric contrast-resolution phantom was developed that can be used for both positive ("hot") and negative contrasts ("cold"). The 3cm long fillable tubes are arranged in six sectors having equal inner diameters ranging from 1mm to 6mm with plastic wall thicknesses of <0.25mm, on a pitch of twice their inner diameters. Scans using simple circular trajectories are first obtained of the activity filled tubes in a uniform water filled cylinder, first with no background activity, and then varying the rod:background concentration ratios from 10:1 to 1:10. The rod phantom is then placed inside a non-uniformly shaped breast phantom and scans are again acquired using both simple and complex 3D trajectories for similarly varying contrasts. Scan times are adjusted to account for radioactive decay, and both low and high noise data is obtained. An iterative OSEM reconstruction algorithm is used to reconstruct the data. Images are evaluated by six independent readers, identifying smallest distinguishable rod for each concentration and experimental setup. Results indicate that, using the SPECT camera having 2.5mm intrinsic pixels, the mean detectable size was ~3.1mm at 10:1 ratio, degrading to ~5.5mm with the 2.5:1 concentration ratio. Furthermore, there was little statistically significant difference ($p<0.05$) between cylinder vs. breast, simple vs. complex trajectories, or whether the rods appeared hot (10:1) or cold (1:10), indicating that data acquisition with the mammotomography system is quite robust.

Introduction

HE dedicated SPECT mammotomography imaging system in our lab allows for fully 3D imaging of a hemispherical volume about a pendant breast, and overcomes several of the physical proximity restrictions of clinical gamma cameras [1-4]. Breast imaging with clinical SPECT cameras is limited by the bulkiness of the large whole body cameras, which results in a larger radius of rotation (ROR). Spatial resolution degrades with increasing distance from the collimator in SPECT, and the larger ROR additionally results in degradation in image quality. The compact gamma camera and flexible system gantry allows close contouring of the pendant, uncompressed breast along with the ability to image lesions close to the chest wall.

With the implementation of this 3D dedicated molecular imaging system, it is necessary to evaluate and characterize system performance to provide tangible motivation for further clinical testing of this paradigm. In previous studies, lesion detectability for varying lesion sizes and contrast ratios has been evaluated using quantitative signal to noise ratio and lesion to background contrast measurements [1, 3, 5]. In order to more fully characterize the system for an object detection imaging task, an observer study is desirable.

Contrast-detail observer studies are commonly used for evaluating imaging system capabilities and have been regularly used for nuclear medicine tomographic and planar imaging systems [6-8]. The goal of this study is to evaluate the minimum object size detectable under a variety of "hot and cold" signal to background contrast ratios since early and later stage, and more and less aggressive cancers take up varying amounts of tracer compounds. Since most cancerous lesions are metabolically active, imaging "hot" lesions is appropriate. Then, as cancers become more advanced, they may contain necrotic cores which do not concentrate radioactive tracers, hence "cold" imaging is also appropriate.

Methods

The compact gamma camera used on our system is the CZT-based *LumaGEM*™ 3200S (*Gamma Medica,* Northridge, CA) with a measured energy resolution of 6.7% FWHM at 140 keV, a sensitivity of 37.9 cps/MBq, and 2.5x2.5mm^2 discrete pixels [3].

Contrast-Detail Phantom Design

A unique geometric contrast-resolution phantom was developed that can be used for both positive ("hot") and negative contrasts ("cold") (Fig. 1). The frame was digitally designed using *Autodesk Inventor* software, and then constructed using 3D stereolithography (*American Precision Prototyping,* Tulsa, OK) using a water resistant resin, DSM

Somos® 11120 (density ~1.12 g/cm^3). The 3cm long thin-walled PTFE plastic tubes (*Small Parts, Inc.*, Miami Lakes, FL) of equal inner diameters (6.2, 5.0, 4.0, 3.1, 2.3, and 1.2mm with wall thicknesses of <0.25mm), on a pitch of twice their inner diameter are arranged in six sectors. For the three smallest diameter sectors, two additional tubes were added, spaced at three times their inner diameter, in order to evaluate if rods were visible at all, regardless of satisfying Nyquist's criteria. Tubes can be independently filled using equal concentrations of activity and then sealed on their open ends with thin plastic tape.

Though loosely based on a mini-cold rod phantom (model ECT/DLX-MP, *Data Spectrum Corp.*, Hillsborough, NC), this phantom can be used for any combination of concentrations; both for hot and cold spot imaging while also varying the background activity and (fluid) composition. The thin wall of the tubes results in minimal scatter and partial volume sampling effects.

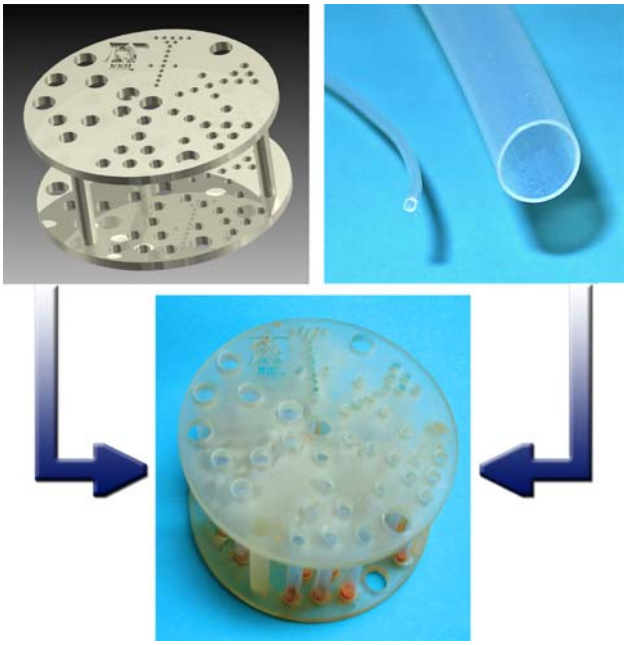

Fig. 1. (TOP LEFT) 3D rendered design of the contrast-detail phantom frame, (TOP RIGHT) Thin-walled PTFE tubing showing two different diameters, (BOTTOM) Completed contrast-detail phantom with tubes glued into the frame. A small amount of modeling clay (orange) was used to prevent leakage in addition to the tape used to seal the tubes.

Rod Phantom in Uniform Cylinder

The first set of experiments was designed to optimally image the phantom using a close ROR (4.3cm), and low scatter conditions. The phantom was placed in a uniform 7.7cm inner diameter cylinder and the background volume was filled with 215ml of water (Fig. 2).

The tubes were individually filled with aqueous [99mTc]-radioactivity with an absolute concentration of 10μCi/ml, while the background was varied, resulting in tube:background ratios of infinite:1, 10:1, 5:1, 2.5:1, 0.4:1, 0.2:1, to 0.1:1. The contrast ratios in this study are modeled

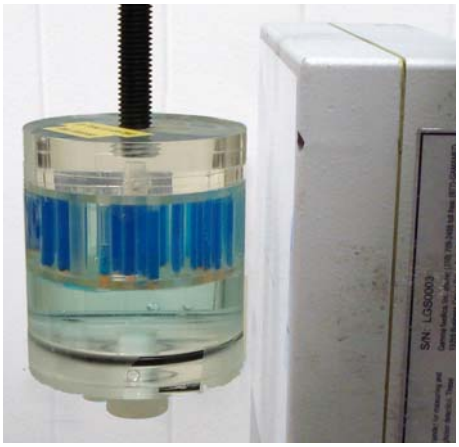

Fig. 2. Contrast-detail phantom in water filled cylinder imaged using a simple circular scan at a close radius of rotation. Blue food coloring was added to the fluid inside the tubes for better visibility.

after clinical findings that [99mTc]-sestamibi concentrates in breast tumors with a mean contrast ratio of ~5.6:1 compared to the surrounding normal tissue, varying from ~2.6:1 up to ~8.7:1 [9].

A vertical axis of rotation 360-degree circular acquisition orbit was used to acquire a total of 128 projections. Scan times were ~10 minutes and then lengthened to account for radioactive decay. Initial count rate was ~300 counts per second (cps) for the 10:1 contrast ratio, thereafter increasing proportional to the added background activity. The energy window used for this and all of the following studies was an 8% (+/- 4) window about the 140keV photopeak.

Rod Phantom in Non-Uniform Breast

The phantom was then placed inside a non-uniformly shaped breast phantom [10], giving more clinically realistic attenuation and scatter characteristics. The breast phantom was filled with 500ml of water to completely submerge the contrast-detail phantom. Scans were obtained using both a simple tilted parallel beam (TPB) and a complex projected sine wave (PROJSINE) 3D trajectory (Fig. 3, Table I). Absolute activity was again 10μCi/ml in the tubes, and activity was continually added to the background to generate the same contrast ratios as for the cylinder experiments. Scan times were again initially 10 minutes and then continually adjusted to account for radioactive decay. Initial count rate was ~480cps for the 10:1 contrast ratio.

TABLE I
PARAMETERS USED FOR BREAST EXPERIMENT ACQUISITIONS OVER A 360° AZIMUTHAL RANGE (θ)

Orbit	Num of Prjs.	Polar Tilt, ϕ (Range, min:max)	ROR (Range, min:max [cm])
TPB	128	45°	6.3
PROJSINE	128	15-45°	3.3-7.6

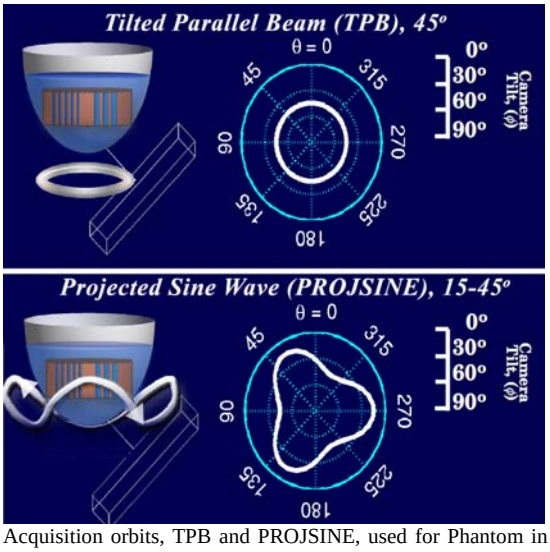

Fig. 3. Acquisition orbits, TPB and PROJSINE, used for Phantom in Breast studies. To the LEFT are visual representations of the 3D orbits and to the RIGHT are polar plots of camera tilt as a function of azimuthal angle, where the radius refers to polar tilt, and in-plane angular displacement represents azimuth.

High Noise Data Set

During data acquisition, noise quality inside the tubes was kept constant for each contrast ratio by adjusting the scan times for radioactive decay. The continually added activity to the background, however, results in a greater number of overall acquired counts, and therefore overall improved noise quality in the background, especially for the "cold" tube:background contrast ratios (0.4:1, 0.2:1, 0.1:1, which correspond to 1:2.5, 1:5, and 1:10, respectively). To account for this in the observer study, a separate set of "high noise" images was created by uniformly, randomly down sampling the breast projection data such that the background noise quality remained constant for each concentration ratio. The total targeted counts in each downsampled projection image were randomly determined using a Poisson distribution with a mean based on the number of counts in each corresponding 10:1 concentration ratio projection image.

Reconstruction and Limited Observer Study

An iterative, ray-driven implemented ordered subsets expectation maximization (OSEM) algorithm, with 8 subsets and 5 iterations was used to accurately model the 3D acquisitions and reconstruct the data. For the phantom breast images, the reconstructed volume was rotated slightly so that the tubes were vertical in the sagittal plane and therefore multiple slices could be combined to enhance image quality. Single planar images were generated for each experiment set by summing planes where rods where present (15 slices) and then smoothing the planar image using the uniform smoothing kernel in *ImageJ*. The images were also rotated clockwise so that the largest diameter rods were in the same position for both the cylinder and breast experiments, in an effort to present unbiased images in the observer study.

The resulting single slice images were evaluated in random order, in a controlled environment by six independent readers, whose task was to identify the smallest distinguishable rods (details) for all concentrations, noise levels and experimental setups and acquisitions.

Results

Rod Phantom in Uniform Cylinder

Vertical circular scans about the phantom in the small cylinder at a minimum ROR represent the best possible imaging conditions for the contrast-detail studies due to the round geometric construction of the phantom with uniform vertical tubes. The entire length of phantom is imaged as near to the camera face as possible at every angle throughout the scan.

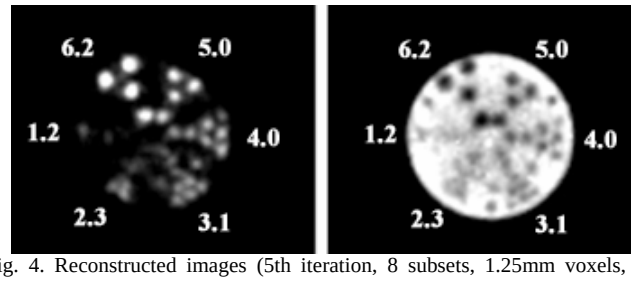

Fig. 4. Reconstructed images (5th iteration, 8 subsets, 1.25mm voxels, 15 summed slices, uniform smoothing) of phantom in cylinder for infinite:1 (LEFT) and 1:10 (RIGHT) concentration ratios. Rod sizes are indicated in mm. Note that three additional cold spots are seen (2, 6, and 10 o'clock) due to the 5mm posts holding the tube alignment layers together.

Reconstructed images from the infinite:1 (no background activity) and 1:10 rod:background concentration ratios (Fig. 4) provide a calibration reference for the other lower contrast and higher scatter and higher noise images (Fig. 5). In Fig. 4 the rods are clearly separable down to the 3.1mm sector for both the hot and cold images, as verified in the observer study results (Fig. 6). It is arguable if the 2.3mm rods are resolvable in the hot image. A small amount of activity leaked out of a few rods potentially contributing to distortion artifacts seen centrally near the 4 and 3.1 mm sectors. A partial matrix of reconstructed images of all contrasts and various acquisition setups is shown in Fig. 5.

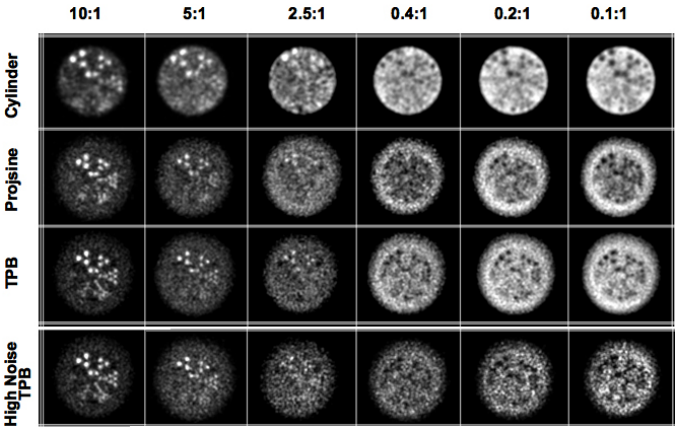

Fig. 5. Reconstructed summed slice images for concentration ratios ranging from 10:1 down to 0.1:1 (effectively 1:10) for circular scans about the cylinder, and two trajectories about the breast phantom. High noise reconstructions for the TPB orbit (only) are shown on the bottom row, where projection count densities were normalized to the 10:1 case.

Observer study results for the cylinder data demonstrate the expected trend that finer resolution is observed for higher contrasts (Fig. 6). The mean observed detail ranges from ~2.2mm in the Inf:1 case, which degrades to ~5.2mm for the 2.5:1 setup, and then inverses from ~4.4mm for the 0.4:1case improving to ~2.7mm for the 0.1:1 concentration ratio.

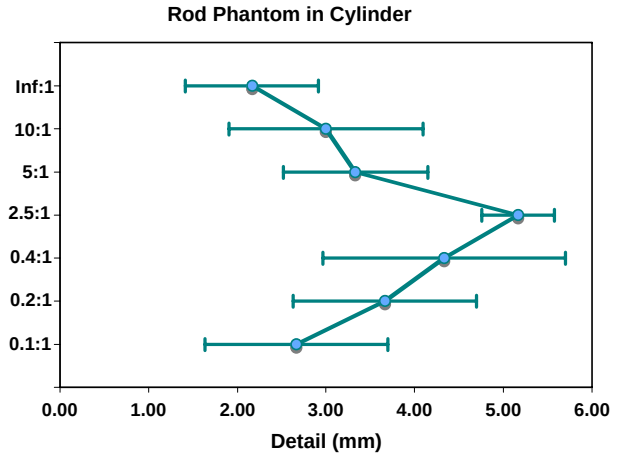

Fig. 6. Contrast vs. detail plot illustrating mean and standard deviation of independent observers.

Student t-test analysis of the cylinder results indicate that resolutions observed for positive and negative contrasts were equivalent, with no statistical differences when comparing hot vs. cold (e.g. 5:1 vs 0.2:1) for any of the contrast ratios.

Rod Phantom in Non-Uniform Breast

The increased background volume of the breast phantom creates an additional scatter medium about the rod phantom, visually apparent in the reconstructed images (Fig. 5). Although the breast phantom used is smaller than the average breast, it represents a clinically more realistic imaging subject than the cylinder.

The mean detectable rod size over all the breast acquisitions was ~3.1mm at the 10:1 concentration ratio, which degraded to ~5.9mm at the 2.5:1 concentration ratio (Figs. 7 and 8). Performance for the rod phantom in the non-uniform breast was therefore very close to that of the rod phantom in the uniform cylinder, with no significant difference at the $p<0.05$ level.

High Vs. Low Noise Images

Though the high noise data sets suffered from a lower number of total counts, observer detection performance remained very close to corresponding lower noise data (Figs. 7 and 8). The only statistically significant differences ($p<0.05$) were at the 2.5:1 concentration ratio for both TPB and PROJSINE data. At the high noise PROJSINE 2.5:1 concentration ratio, no rods were discernable by any of the readers, and thus a data point is not placed on the contrast-detail plot.

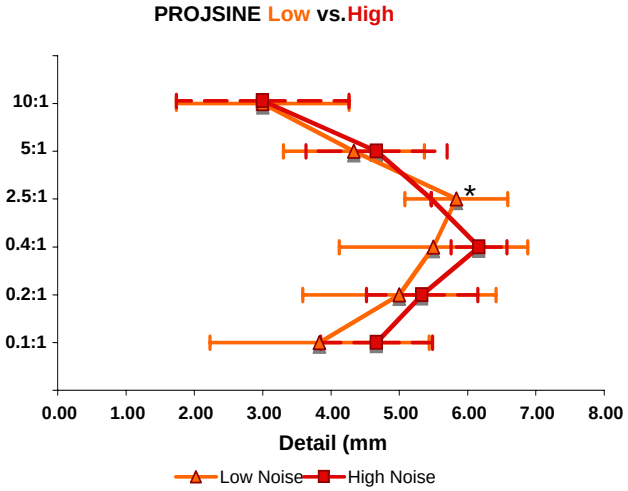

Since images are smoothed clinically before they are viewed, a modest amount of smoothing was used on all image sets. Summing multiple slices and smoothing the reconstructed images likely improved the observer results, especially for the high noise images. Though a slight separation in mean values between low and high noise data sets exists, the observer study results are promising for clinical applications where detected count densities are more similar to the high noise data.

Fig. 7. Contrast vs. detail plots comparing low vs. high noise data sets for PROJSINE trajectory about the breast phantom. Asterisk denotes statistically significant differences (at $p<0.05$).

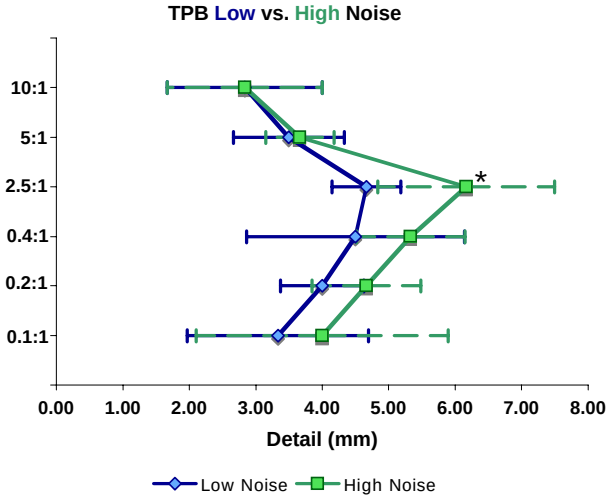

Fig. 8. Contrast vs. detail plots comparing low vs. high noise data sets for TPB orbit about the breast phantom. Asterisk denotes statistically significant differences in mean values (at $p<0.05$).

PROJSINE vs. TPB Trajectories

Because there was little statistical variation in detection results between the low and high noise images, the two

observation sets were combined to compare performance between the two acquisition orbits (Fig 9). The TPB demonstrated significantly ($p<0.05$) finer resolution for the 5:1 and 2.5:1 cases. This is likely due to the fact that the TPB acquisition orbit contained many views at a closer proximity to the phantom, while PROJSINE moved farther from the rods due to variations in both polar angle and radius of rotation (Table I).

Traditional hot rod (infinite:1 contrast) and, inversely, cold rod scans were acquired using the PROJSINE orbit yielding mean observed values of ~2.4mm for Inf:1 and ~3.1mm for 1:Inf.

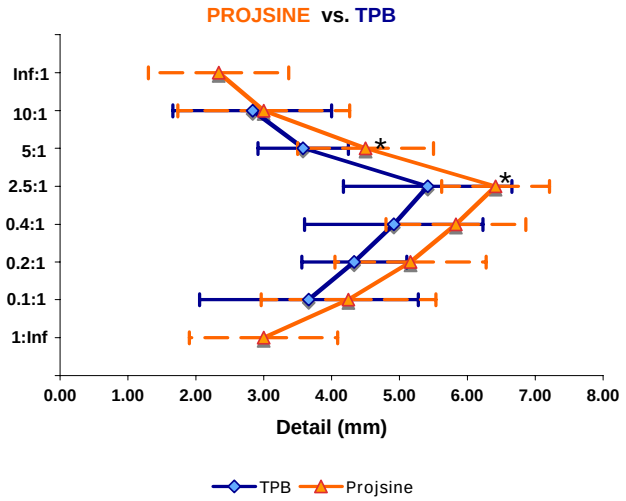

Fig. 9. Contrast vs. detail comparing PROJSINE to TPB trajectories using combined high and low noise observations. Asterisks denote statistically significant differences in mean values at $p<0.05$. For the Inf:1, and 1:Inf concentration ratios, only PROJSINE scans were acquired.

Conclusions

A novel contrast-detail phantom was designed, constructed, and successfully used for evaluation of the dedicated emission mammography system. Results of a contrast-detail observer study indicate that, using the SPECT camera having 2.5mm intrinsic pixels, the mean detectable size over all the experiments was ~3.1mm at a 10:1 ratio, degrading to ~5.5mm with the 2.5:1 concentration ratio. Student t-tests showed little statistical significance between the higher vs. lower count densities. Resolution was proportional to the radius of rotation of the camera, highlighted for example by the observed finer resolution at 5:1 and 2.5:1 for TPB vs. Projsine scans because TPB contained more views at a closer proximity to the phantom. Furthermore, there was little statistically significant difference ($p<0.05$) between cylinder vs. breast, simple vs. complex trajectories, or whether the rods appeared hot (10:1) or cold (1:10), indicating that data acquisition with the mammotomography system is quite robust.

For improved accuracy, a larger sample set of images is needed to more completely characterize the system. More realistic, 3D spherical lesions should be evaluated at various contrasts for variety of breast sizes in a broader observer study, since there are advantages here of summing multiple reconstructed image planes of the symmetric rods. The developed contrast-detail phantom will, however, be useful for a variety of other applications, such as for SPECT/CT multi-modality imaging and co-registration, by placing aqueous activity in the tubes and replacing the background liquid with fluids of varying density to modify the CT contrast.

Acknowledgment

The authors thank Dominic Crotty, Randy McKinley, Priti Madhav, and Brooke Cutler for their assistance and participation in the observer study.

References

[1] C. N. Archer, M. P. Tornai, J. E. Bowsher, S. D. Metzler, B. C. Pieper, and R. J. Jaszczak, "Implementation and initial characterization of acquisition orbits with a dedicated emission mammotomograph," *IEEE Trans. Nucl. Sci.*, vol. 50, pp. 413-420, 2003.

[2] M. P. Tornai, J. E. Bowsher, C. N. Archer, J. Peter, R. J. Jaszczak, L. R. MacDonald, B. E. Patt, and J.S. Iwanczyk, "A 3D Gantry Single Photon Emission Tomograph with Hemispherical Coverage for Dedicated Breast Imaging," *Nucl. Instr. Meth. Phys. Res. A*, vol. 497, pp. 157-167, 2003.

[3] C. N. Brzymialkiewicz, M. P. Tornai, R. L. McKinley, and J. E. Bowsher, "Evaluation of Fully 3D Emission Mammotomography with a Compact Cadmium Zinc Telluride Detector," *IEEE Trans. Med. Imag.*, vol. 24, pp. 868-877, 2005.

[4] C. N. Brzymialkiewicz, M. P. Tornai, R. L. McKinley, S. J. Cutler, and J. E. Bowsher, "Performance of dedicated emission mammotomography for various breast shapes and sizes," *Physics in Medicine and Biology*, vol. 51, pp. 5051-5064, 2006.

[5] M. P. Tornai, C. N. Brzymialkiewicz, M. L. Bradshaw, J. E. Bowsher, B. E. Patt, J. S. Iwanczyk, J. Li, and L. R. MacDonald, "Comparison of compact gamma cameras with 1.3- and 2.0-mm quantized elements for dedicated emission mammotomography," *Nuclear Science, IEEE Transactions on*, vol. 52, pp. 1251-1256, 2005.

[6] K. Faulkner and B. M. Moores, "Contrast-detail assessment of computed tomographic scanners," *Phys. Med. Biol.*, vol. 31, pp. 993-1003, 1986.

[7] D. P. McElroy, E. J. Hoffman, L. MacDonald, B. E. Patt, J. S. Iwanczyk, Y. Yamaguchi, and C. S. Levin, "Evaluation of breast tumor detectability with two dedicated, compact scintillation cameras," *Nuclear Science, IEEE Transactions on*, vol. 49, pp. 794-802, 2002.

[8] M. J. More, P. J. Goodale, S. Majewski, and M. B. Williams, "Evaluation of Gamma Cameras for Use in Dedicated Breast Imaging," *Nuclear Science, IEEE Transactions on*, vol. 53, pp. 2675-2679, 2006.

[9] J. Maublant, M. de Latour, D. Mestas, A. Clemenson, S. Charrier, V. Feillel, G. Le Bouedec, P. Kaufmann, J. Dauplat, and A. Veyre, "Technetium-99m-sestamibi uptake in breast tumor and associated lymph nodes," *J Nucl Med*, vol. 37, pp. 922-5, Jun 1996.

[10] M. P. Tornai, R. L. McKinley, C. N. Bryzmialkiewicz, S. J. Cutler, and D. J. Crotty, "Anthropomorphic breast phantoms for preclinical imaging evaluation with transmission or emission imaging," in *Proc. SPIE: Phys. Med. Imag.*, San Diego, CA, USA, 2005, pp. 825-834.

Appendix C

Empirical Effects of Angular Sampling and Background Content on Image Quality in Dedicated Breast SPECT

Kristy L Perez[1,2], Spencer J Cutler[1,3], Martin P Tornai[1,2,3]

[1] *Department of Radiology, Duke University Medical Center, Durham, NC 27710*
[2] *Medical Physics Graduate Program, Duke University, Durham, NC 27710*
[2] *Department of Biomedical Engineering, Duke University, Durham, NC 27708*

This study investigates the importance and effects of varying the azimuthal and polar sampling of the acquisition trajectory with the dedicated breast SPECT imaging system developed in our lab. In addition, the frequency quality (density and distribution) of the background is considered. The SPECT system consists of a 16x20cm^2 CZT gamma camera with 6.7% FWHM energy resolution at 140keV, which can accommodate fully 3D simple or complex trajectories about a pendant, uncompressed breast. Various geometric and anthropomorphic phantoms containing lesions are imaged to evaluate the effects of sampling and background distributions on signal (lesion) visualization. In one initial study, two lesions (~0.2 and 0.4ml) are positioned in approximately the same location inside a uniformly filled breast phantom with constant background activity for a variety of angular sampling tests. Evaluated lesion SNR and contrast demonstrated greater effect due to the number of counts per projection than the total number of projections, but this only considered a uniform background signal content. Additionally, azimuthal sampling impacted signal intensity to a greater degree than polar sampling. Additional detailed statistical studies of the angular sampling in the azimuthal and polar directions to characterize the system are underway. Orbits with a variety of projection numbers (64, 128 and 256) and polar tilts (constant, 45° range and 30° range) are being tested with lesions scanned in air and a variety of background activities and density distribution (non-uniform) conditions. In general, sufficient counting statistics limit the quality of the image and thus an optimization between the number of projections and the number of detected events is being explored.